

Optimization-based method for conjugate heat transfer problems

Liang Fang¹, Xiandong Liu², Lei Zhang².

¹ School of Automotive Studies, Tongji University, Shanghai 201804, China, fangliang@tongji.edu.cn

² School of Mathematical Sciences, Key Laboratory of Intelligent Computing and Applications (Ministry of Education), Tongji University, Shanghai 200092, China, 2333706@tongji.edu.cn, 22210@tongji.edu.cn

Abstract

We propose a numerical approach for solving conjugate heat transfer problems using the finite volume method. This approach combines a semi-implicit scheme for fluid flow, governed by the incompressible Navier-Stokes equations, with an optimization-based approach for heat transfer across the fluid-solid interface. In the semi-implicit method, the convective term in the momentum equation is treated explicitly, ensuring computational efficiency, while maintaining stability when a CFL condition involving fluid velocity is satisfied. Heat exchange between the fluid and solid domains is formulated as a constrained optimization problem, which is efficiently solved using a sequential quadratic programming method. Numerical results are presented to demonstrate the effectiveness and performance of the proposed approach.

Keywords: conjugate heat transfer; optimization-based method; partitioned method; incompressible Navier-Stokes equations; semi-implicit method; finite volume methods

1 Introduction

Conjugate heat transfer (CHT) problems, which involve the thermal interaction of fluid and solid domains, are prevalent in a wide range of science and engineering applications. These include cooling system analysis [1] and turbocharger modeling [2] in automotive engineering, transonic nozzle flow simulation in aerospace engineering [3], electronic device cooling [4, 5] etc. Developing efficient and robust numerical methods for solving CHT problems is essential for the design, optimization, performance evaluation, and safety analysis of various industrial systems.

Two predominant approaches are commonly employed in the numerical treatment of CHT problems: the monolithic and partitioned methods. The monolithic approach [6, 7, 8] treats the fluid and solid governing equations as a single coupled system, offering superior convergence properties and stability. However, its lack of flexibility is a major drawback, as it does not allow the use of existing solvers independently for the fluid and solid sub-problems. In contrast, the partitioned approach [9, 10, 11, 12] separates the treatment of the fluid and solid sub-problems by solving each domain independently and iterating between them to enforce the fluid-solid interface conditions. This strategy benefits from the use of established solvers for both sub-problems, offering greater flexibility and ease of implementation.

Partitioned methods differ in their approach to enforcing the interface conditions. One of the most commonly used iterative techniques is the Dirichlet-to-Neumann (DtN) approach [13, 14, 11, 15]. In this method, a Dirichlet boundary condition is imposed at the fluid-solid interface for the fluid sub-problem to ensure temperature continuity, while the solid sub-problem is governed by a Neumann boundary condition at the interface to maintain heat flux continuity. Alternatively, the roles of these boundary conditions can be reversed, depending on the thermal effusivities of the fluid and solid, to ensure stability [16]. The efficiency of partitioned schemes can be improved by exchanging boundary conditions only after multiple time steps on the fluid and solid domains, to guarantee a fast convergence of the coupled problem [11]. Additionally, variants such as the Dirichlet-Robin iterative method [12, 17] have been proposed to further enhance stability and convergence, especially in fluid-solid coupling involving high Biot numbers. Furthermore, adaptive coupling coefficients have been introduced to optimize CHT for improved stability [18].

In partitioned approaches for CHT problems, the fluid flow needs to be solved multiple times per time step with varying fluid-solid interface conditions due to the iterative thermal exchange between fluid and solid domains. Thus, the efficiency of the numerical solver for fluid flow, governed by the Navier-Stokes equations, is crucial. Pressure-based methods, such as the SIMPLE-family algorithms [19, 20], are widely used for solving incompressible fluid flows. These methods rely on a prediction-correction procedure and provide a reliable and efficient approach for CHT simulations [6, 21, 3]. Other efficient solvers include the coupled method proposed in [22], which enhances computational performance by solving for pressure and velocity simultaneously, in contrast to the typical sequential approach where the momentum and pressure correction equations are solved separately. Additionally, semi-implicit methods [23, 24] offer an efficient approach to solving the Euler equations

in the context of two-phase compressible flows. Furthermore, fully decoupled monolithic projection methods [7, 8] linearize the nonlinear convective term and rely on approximate factorization techniques, ensuring stability and computational efficiency.

The objective of this work is to propose an efficient partitioned numerical framework for solving CHT problems. To this end, we integrate a semi-implicit method for fluid flow with an optimization-based approach for heat transfer across the fluid-solid interface. The semi-implicit method solves the Navier-Stokes equations governing the fluid flow, treating the convective term in the momentum equation explicitly to ensure computational efficiency, while maintaining stability under a Courant-Friedrichs-Lewy (CFL) condition constrained by the fluid velocity. The stability condition is rigorously established through von Neumann analysis. By eliminating sub-iterations within each time step, this approach significantly enhances computational performance for time-dependent problems. For heat transfer, we reformulate the coupling problem as a constrained optimization problem. While optimization-based approaches have been proposed within the finite element framework for domain decomposition problems [25, 26], in this study, we extend this concept to the finite volume discretization framework. The resulting optimization problem is efficiently solved using a sequential quadratic programming (SQP) method [27]. When applying the SQP method, the computation of the Jacobian matrix, which involves differentiating the sub-problem residual with respect to the control variable, is computationally expensive. This issue becomes particularly pronounced when the number of interface faces is large. To mitigate this computational cost, we introduce a reduced representation of the interface [28, 29] to further enhance the efficiency of the optimization-based method.

This paper is organized as follows. Section 2 introduces the governing equations considered in this work. Section 3 details the semi-implicit method for fluid flow, the optimization-based approach for heat transfer, and their integration in CHT problems. Section 4 presents numerical results to validate the proposed numerical framework and to illustrate its properties.

2 Governing equations

In this section, we present the governing equations for CHT problems [14, 10, 8]. A schematic representation of the computational domain is shown in Figure 1.

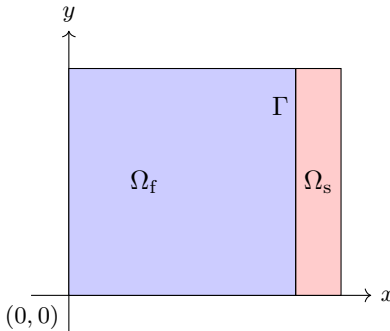


Figure 1: computational domain for conjugate heat transfer.

The fluid domain Ω_f is governed by the incompressible Navier-Stokes equations for fluid flow and an advection-diffusion equation for temperature (energy equation):

$$\nabla \cdot \mathbf{u}_f = 0, \quad (1)$$

$$\rho_f \frac{\partial \mathbf{u}_f}{\partial t} + \nabla \cdot (\rho_f \mathbf{u}_f \otimes \mathbf{u}_f) = \nabla \cdot (\mu_f \nabla \mathbf{u}_f) - \nabla p - \rho_f \beta \mathbf{g}_0 (T_f - T_{\text{ref}}), \quad (2)$$

$$\rho_f c_{\text{pf}} \left(\frac{\partial T_f}{\partial t} + \nabla \cdot (\mathbf{u}_f T_f) \right) = \nabla \cdot (k_f \nabla T_f) + Q_f, \quad (3)$$

where \mathbf{u}_f is the velocity field, p is the pressure, ρ_f is the fluid density, μ_f is the dynamic viscosity, T_f is the fluid temperature, k_f is the thermal conductivity, c_{pf} is the specific heat capacity, Q_f represents the heat source in the fluid, β is the thermal expansion coefficient of the fluid, and \mathbf{g}_0 is the gravitational acceleration. The term $\rho_f \beta \mathbf{g}_0 (T_f - T_{\text{ref}})$ represents buoyancy effects under the Boussinesq approximation. If buoyancy effects are neglected, the energy equation becomes decoupled from the mass and momentum equations.

Heat transfer in solid domain Ω_s is governed by the heat conduction equation:

$$\rho_s c_{\text{ps}} \frac{\partial T_s}{\partial t} = \nabla \cdot (k_s \nabla T_s) + Q_s, \quad (4)$$

where T_s is the temperature field in the solid, k_s is the thermal conductivity, ρ_s and c_{ps} are the density and specific heat, and Q_s is the source term.

At the fluid-solid interface Γ , the following conjugate boundary conditions enforce continuity of temperature and heat flux:

$$\begin{aligned} T_s &= T_f, \\ k_s \frac{\partial T_s}{\partial \mathbf{n}} &= k_f \frac{\partial T_f}{\partial \mathbf{n}}, \end{aligned} \quad (5)$$

where \mathbf{n} is the unit normal vector at the interface, pointing from the fluid domain to the solid domain.

3 Numerical methods

3.1 Semi-implicit method for the Navier-Stokes equations

In this section, we present a semi-implicit finite volume method for solving the incompressible Navier-Stokes equations. This method is designed for unsteady problems, where the convective term is treated explicitly. The pressure and diffusion terms are handled implicitly to ensure that the time step is limited by the fluid flow velocity. By explicitly treating the nonlinear convective term, the method theoretically eliminates the need for sub-iterations to address non-linearity, unlike projection-based approaches such as the SIMPLE method. Consequently, the semi-implicit method offers computational efficiency for time-dependent problems. A similar semi-implicit approach has been previously considered in the context of compressible two-phase flows [24] using the Euler equations, where the diffusion term was not included. Here, we apply the semi-implicit method to incompressible flows and incorporate the diffusion term. In this study, we consider first-order time and spatial discretization.

Here, we consider the case where the energy equation is decoupled, meaning that we solve the Navier-Stokes equations (1)-(2) while neglecting the buoyancy term in the momentum equation (2). The treatment of the fully coupled system (1)-(5), which includes the energy equation and the coupling with the solid, will be addressed in Section 3.3. We integrate the momentum and mass equations over a control volume C using the finite volume method, leading to the discretized Navier-Stokes equations:

$$\rho_f \frac{(\mathbf{u}_f)_C^{n+1} - (\mathbf{u}_f)_C^n}{\Delta t} + \frac{1}{V_C} \sum_{b(C)} (\rho_f \mathbf{u}_f)_b^n [(\mathbf{u}_f)_b^n \cdot \mathbf{S}_{f,b}] = -\nabla P_C^{n+1} + \frac{1}{V_C} \sum_{b(C)} (\mu_f \nabla \mathbf{u}_f)_b^{n+1} \cdot \mathbf{S}_{f,b}, \quad (6)$$

$$\sum_{b(C)} (\mathbf{u}_f)_b^{n+1} \cdot \mathbf{S}_{f,b} = 0, \quad (7)$$

where $b(C)$ denotes the boundary of cell C , the subscript $(\cdot)_b$ indicates the value at cell boundary b , and the area vector $\mathbf{S}_{f,b}$ is defined as $\mathbf{S}_{f,b} = \mathbf{n}_{f,b} A_{f,b}$, i.e., the unit normal vector $\mathbf{n}_{f,b}$ scaled by the area of the cell boundary b . The transported quantity $(\rho_f \mathbf{u}_f)_b^n$ is determined using the upwind scheme, and the diffusion term $(\mu_f \nabla \mathbf{u}_f)_b^{n+1}$ can be related to the velocities of the two adjacent cells of the boundary face b using standard techniques (cf. [20, chap. 8]).

The discretized momentum equation (6) can be rewritten in the following compact form

$$a_C (\mathbf{u}_f)_C^{n+1} + \sum_{F \in \text{nb}(C)} a_F (\mathbf{u}_f)_F^{n+1} = -\nabla P_C^{n+1} + \mathbf{B}_C^n, \quad (8)$$

where $\text{nb}(C)$ denotes the neighboring cells of cell C . This compact form is exploited in B to derive an iterative procedure to solve the above discretized system.

The discretized system (6)-(7) is further complemented by the Rhie-Chow interpolation [30], which determines the fluid velocity at the cell face $(\mathbf{u}_f)_b^{n+1}$ in the mass conservation equation (7). Specifically, the face velocity is computed as

$$(\mathbf{u}_f)_b^{n+1} = \frac{1}{2} [(\mathbf{u}_f)_C^{n+1} + (\mathbf{u}_f)_{C'}^{n+1}] - (\mathbf{D}_f)_b [(\nabla P)_b^{n+1} - \overline{(\nabla P)_b^{n+1}}], \quad (9)$$

where C and C' are the two adjacent cells of face b ; $(\mathbf{D}_f)_b = \frac{1}{2} [(\mathbf{D}_f)_C + (\mathbf{D}_f)_{C'}]$, $(\mathbf{D}_f)_C = 1/a_C$, $(\mathbf{D}_f)_{C'} = 1/a_{C'}$; $\overline{(\nabla P)_b^{n+1}}$ is the average of the pressure derivatives of the two adjacent cells. In this work, we consider only orthogonal grids. For non-orthogonal grids, various correction techniques [24][20, chap. 8]) can be employed, we omit the details for brevity.

The global system based on equations (7)-(9) can be formulated as a linear system, with $(\mathbf{u}_f)_C^{n+1}$, P_C^{n+1} , $(\mathbf{u}_f)_b^{n+1}$ as the unknowns. We present the following theorem, which establishes that the semi-implicit method remains stable provided that the Courant-Friedrichs-Lewy (CFL) condition, determined by the flow velocity, is satisfied.

Theorem 1. *The semi-implicit method, with Rhie-Chow interpolation for computing the face velocity, is stable if the CFL condition is satisfied:*

$$0 \leq C_m \leq 1, \quad (10)$$

where $C_m = C_{m1} + C_{m2} = \frac{u_0 \Delta t}{\Delta x} + \frac{v_0 \Delta t}{\Delta y}$, u_0 and v_0 represent the characteristic flow velocities in the x - and y -directions, respectively, Δx and Δy denote the spatial discretization sizes in the x - and y -directions, and Δt is the time step.

The proof of Theorem 1 is provided in A. Since the global system is linear, standard linear solvers can be applied directly to solve it without subiterations. However, in B we introduce a preliminary iterative method solver for the global problem, employing a prediction-correction approach similar to the SIMPLE method. Unlike the SIMPLE method, the matrices to be solved in the prediction step and for the pressure correction equation remain unchanged across sub-iterations and time steps. This characteristic can be leveraged to further improve the efficiency of the overall algorithm. The resolution of the global system (7)-(9) using more efficient techniques such as matrix factorization techniques similar to those in [7, 31] is subject of future research.

3.2 Optimization-based method for heat transfer problems

We introduce an optimization-based method to solve the heat transfer problem defined by equations (3)–(4), subject to the coupling conditions given in (5). In this section, we assume that the fluid velocity, \mathbf{u}_f , is known. The case where the fluid velocity is also treated as an unknown variable will be addressed in the subsequent section.

The integration of the temperature equations for the fluid and the solid over control volumes C_f and C_s , respectively, yields the following equations:

$$\rho_f c_{pf} \left[\frac{T_f^{n+1} - T_f^n}{\Delta t} + \frac{1}{V_{C_f}} \sum_b (\mathbf{u}_{f,b} \cdot \mathbf{S}_{f,b}) T_{f,b}^{n+1} \right] = \frac{1}{V_{C_f}} \sum_b \left(k_{f,b} \nabla T_{f,b}^{n+1} \cdot \mathbf{S}_{f,b} \right) + Q_f, \quad (11)$$

$$\rho_s c_{ps} \frac{T_s^{n+1} - T_s^n}{\Delta t} = \frac{1}{V_{C_s}} \sum_b \left(k_{s,b} \nabla T_{s,b}^{n+1} \cdot \mathbf{S}_{s,b} \right) + Q_s. \quad (12)$$

Here, the area vector $\mathbf{S}_{f,b}$ is defined as in Section 3.1, and $\mathbf{S}_{s,b}$ is defined in a similar manner. We distinguish between two types of cell boundaries: (1) internal boundaries or domain boundaries that do not involve the fluid-solid interface, and (2) boundaries corresponding to the fluid-solid interface. For the first type of cell boundary, standard numerical strategies can be applied to handle the associated terms. Specifically, the convective term in the fluid equation at the cell boundary $T_{f,b}^{n+1}$ can be determined using an upwind scheme or by applying appropriate boundary conditions. The diffusion terms at the cell boundary, $\nabla T_{f,b}^{n+1}$ and $\nabla T_{s,b}^{n+1}$, can be related to the temperatures of the two adjacent cells at the boundary face b using standard techniques (cf. [20, chap. 8]), or by applying the appropriate treatment of boundary conditions.

For a cell boundary of type (2), i.e., a boundary that lies on the fluid-solid interface (cf. Figure 2, where the cell boundary b located at the interface), the contribution of the cell boundary to the convective term in the fluid equation is zero, as we assume a no-slip wall condition at the interface. Regarding the diffusion term, the coupling condition (5)₂ and the assumption of a conforming mesh ensure that the heat flux remains continuous across the interface, leading to the equality $k_{f,b} \nabla T_{f,b}^{n+1} \cdot \mathbf{S}_{f,b} = -k_{s,b} \nabla T_{s,b}^{n+1} \cdot \mathbf{S}_{s,b}$. We denote this common heat flux across the interface face b as g_b^{n+1} , such that:

$$g_b^{n+1} = k_{f,b} \nabla T_{f,b}^{n+1} \cdot \mathbf{S}_{f,b} = -k_{s,b} \nabla T_{s,b}^{n+1} \cdot \mathbf{S}_{s,b}. \quad (13)$$

This formulation leads to the following algebraic equations in compact form for the heat transfer equations in the fluid and solid subdomains:

$$\mathbf{R}_f(\mathbf{T}_f^{n+1}) - \mathbf{E}_f \mathbf{g}^{n+1} = 0, \quad (14)$$

$$\mathbf{R}_s(\mathbf{T}_s^{n+1}) + \mathbf{E}_s \mathbf{g}^{n+1} = 0, \quad (15)$$

where $\mathbf{T}_f^{n+1} \in \mathbb{R}^{N_f}$ and $\mathbf{T}_s^{n+1} \in \mathbb{R}^{N_s}$ represent the temperature vectors at the cell center for all cells in the fluid and solid domains, respectively. Here, N_f and N_s denote the number of cells in the fluid and solid domains. The residuals $\mathbf{R}_f \in \mathbb{R}^{N_f}$ and $\mathbf{R}_s \in \mathbb{R}^{N_s}$ may be nonlinear, for example, when temperature-dependent diffusion coefficients k_f and k_s are considered. The vector $\mathbf{g} \in \mathbb{R}^{N_\Gamma}$ represents the heat flux across all faces of the interface, where N_Γ is the total number of interface faces. In accordance with the discretized equation (11), the matrix $\mathbf{E}_f \in \mathbb{R}^{N_f \times N_\Gamma}$ in the coupling term is constructed as follows: $(\mathbf{E}_f)_{ij} = 1$ if the j -th face belongs to the i -th cell, and $(\mathbf{E}_f)_{ij} = 0$ otherwise. The construction for $\mathbf{E}_s \in \mathbb{R}^{N_s \times N_\Gamma}$ follows similarly.

Note that given the flux at the fluid-structure interface \mathbf{g} , the fluid and solid sub-problems can be decoupled and fully determined independently. As described in [25, 26, 27], we refer to \mathbf{g} as the control. However, an

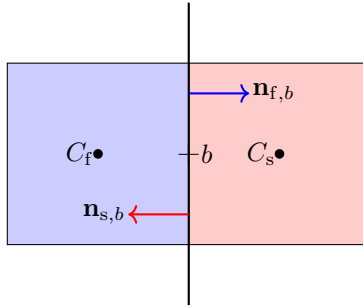


Figure 2: illustration of fluid-solid interface with two adjacent cells.

arbitrary choice of the control \mathbf{g} does not guarantee that the local solutions to (14)-(15) satisfy the transmission condition (5)₁ and hence will not be valid solutions to the coupled problem (3) and (4). The *optimal control* \mathbf{g} that guarantees temperature continuity at the interface Γ can be obtained by solving the following optimization problem

$$\min_{\substack{\mathbf{T}_f^{n+1}; \\ \mathbf{T}_s^{n+1}; \\ \mathbf{g}^{n+1}}} F_\delta(\mathbf{T}_f^{n+1}, \mathbf{T}_s^{n+1}, \mathbf{g}^{n+1}) := \frac{1}{2} \left\| \mathbf{T}_{f,\Gamma}^{n+1} - \mathbf{T}_{s,\Gamma}^{n+1} \right\|_2^2 + \frac{\delta}{2} \|\mathbf{g}^{n+1}\|_2^2, \quad (16)$$

with equations (14) and (15) as constraints. Here, $\mathbf{T}_{f,\Gamma}^{n+1}$ and $\mathbf{T}_{s,\Gamma}^{n+1}$ represent the temperature at all faces of the interface Γ for the fluid and solid domains, respectively. The second term in the objective function of (16) is a regularizer, designed to penalize controls of excessive size; the positive constant δ is selected to control the relative importance of the two terms in the objective function. The optimization-based methodology has been effectively applied to domain-decomposition problems involving elliptic equations [32] and Navier-Stokes equations [26, 27] within the framework of finite-element methods. In this work, we extend this methodology to the context of finite-volume methods for addressing multiphysics problems.

In the optimization formula, the temperature at the interface is required in the objective function (16). However, in the context of finite volume methods, the resolution of the local subproblems (14)-(15) gives the temperature at the cell center rather than directly at the cell face. We now describe how the temperature at the interface can be determined using the heat flux \mathbf{g} . The directional gradient of the temperature along the normal at the interface boundary b (cf. Figure 2) can be determined as

$$\nabla T_{f,b}^{n+1} \cdot \mathbf{n}_{f,b} = \frac{g_b^{n+1}}{k_{f,b} A_{f,b}},$$

for the fluid, and similarly for the solid

$$\nabla T_{s,b}^{n+1} \cdot \mathbf{n}_{s,b} = \frac{-g_b^{n+1}}{k_{s,b} A_{s,b}},$$

where these expressions follows directly from the definition of g_b^{n+1} in equation (13). The temperature at the interface can now be determined using these gradients and the temperature at the cell center as

$$T_{f,b}^{n+1} = \nabla T_{f,b}^{n+1} \cdot \mathbf{n}_{f,b} d_{b,C_f} + T_{C_f}^{n+1},$$

where d_{b,C_f} is the distance between the cell center C_f and the face center b . This relation can be established for all faces of the interface, and finally we obtain the temperature at the interface in vector form

$$\mathbf{T}_{f,\Gamma}^{n+1} = \frac{\mathbf{g}^{n+1}}{\mathbf{k}_{f,\Gamma} \mathbf{A}_{f,\Gamma} / \mathbf{d}_{f,\Gamma}} + \mathbf{T}_f^{n+1}|_\Gamma, \quad (17)$$

where $\mathbf{k}_{f,\Gamma}$, $\mathbf{A}_{f,\Gamma}$, $\mathbf{d}_{f,\Gamma}$ represent the vectorized thermal conductivity, face area, and distance between the face center and the corresponding cell center, for all faces of the interface; $\mathbf{T}_f^{n+1}|_\Gamma$ denotes the restriction of \mathbf{T}_f^{n+1} to cells that share a face at the interface. A similar expression can be obtained for the solid:

$$\mathbf{T}_{s,\Gamma}^{n+1} = \frac{\mathbf{g}^{n+1}}{\mathbf{k}_{s,\Gamma} \mathbf{A}_{s,\Gamma} / \mathbf{d}_{s,\Gamma}} + \mathbf{T}_s^{n+1}|_\Gamma. \quad (18)$$

3.2.1 Sequential quadratic programming method for solving the optimization problem

We resort to the sequential quadratic programming (SQP) method [27] to solve the constrained optimization problem, which involves the linearization of the nonlinear constraints. Given the relations (17)-(18), which link

the temperature at cell face and the temperature at cell center, we solve the following optimization problem at each SQP iteration:

$$\min_{\mathbf{T}_f, \mathbf{T}_s, \mathbf{g}} F_\delta(\mathbf{T}_f, \mathbf{T}_s, \mathbf{g}) := \frac{1}{2} \left\| (\mathbf{T}_f - \mathbf{T}_s)|_\Gamma + \mathbf{g} \left(\frac{1}{\mathbf{k}_{f,\Gamma} \mathbf{A}_{f,\Gamma} / \mathbf{d}_{f,\Gamma}} + \frac{1}{\mathbf{k}_{s,\Gamma} \mathbf{A}_{s,\Gamma} / \mathbf{d}_{s,\Gamma}} \right) \right\|_2^2 + \frac{\delta}{2} \|\mathbf{g}\|_2^2, \quad (19)$$

subject to the linearized constraints

$$\begin{cases} \mathbf{R}_f^{n+1,k} + \mathbf{J}_f^{n+1,k}(\mathbf{T}_f - \mathbf{T}_f^{n+1,k}) - \mathbf{E}_f \mathbf{g} = 0, \\ \mathbf{R}_s^{n+1,k} + \mathbf{J}_s^{n+1,k}(\mathbf{T}_s - \mathbf{T}_s^{n+1,k}) + \mathbf{E}_s \mathbf{g} = 0, \end{cases} \quad (20)$$

where k denotes the SQP iteration number, $\mathbf{R}_f^{n+1,k}$ and $\mathbf{R}_s^{n+1,k}$ are the residuals evaluated at $\mathbf{T}_s^{n+1,k}$, $\mathbf{T}_s^{n+1,k}$, respectively; the Jacobian matrices $\mathbf{J}_f^{n+1,k}$ and $\mathbf{J}_s^{n+1,k}$ represent the derivatives of the residuals $\mathbf{R}_f^{n+1,k}$ and $\mathbf{R}_s^{n+1,k}$ with respect to the temperature evaluated at iteration k , $\mathbf{T}_s^{n+1,k}$, $\mathbf{T}_s^{n+1,k}$. The linearized constraints lead to a relationship between \mathbf{T}_f , \mathbf{T}_s and the control \mathbf{g} . By substituting these relations in the objective function (19), we obtain a least-squares problem for the control \mathbf{g} , which can be solved efficiently using the Gauss-Newton method [33, chap. 10]. The SQP method converges as long as the difference in \mathbf{g} between two successive SQP iterations is below a predefined threshold, which allows to proceed to the next time step.

Remark 3.1. *One of the most commonly used approaches for solving CHT problems is the Dirichlet-to-Neumann (DtN) method [11]. In this method, the temperature is computed on the solid side of the interface and used as a Dirichlet boundary condition for the fluid domain; subsequently, the heat flux is calculated on the fluid side and applied as a Neumann boundary condition on the solid side; or vice versa. This procedure is inherently sequential and relies on alternating boundary conditions between the two subdomains. In contrast, the optimization-based (OB) method offers a parallel approach by introducing a control variable, \mathbf{g} , which represents the heat flow across the interface. In this formulation, both subdomains are treated with Neumann boundary conditions. The coupling condition for the continuity of heat flux is inherently satisfied, while the continuity of temperature is ensured by solving the optimization problem (16). In Section 4, we compare the performance of the DtN method and the OB method, highlighting the efficiency of the OB method.*

3.2.2 Reduced optimization-based method

In applying the SQP method to solve the optimization problem, each SQP iteration requires the computation of $(\mathbf{J}_f^{n+1,k})^{-1} \mathbf{E}_f$ and $(\mathbf{J}_s^{n+1,k})^{-1} \mathbf{E}_s$, which can be computationally expensive, especially when the number of faces at the interface is large. To improve the efficiency of the SQP method, we adopt a reduced representation of the control as follows:

$$\mathbf{g} = \Phi \boldsymbol{\beta}, \quad (21)$$

where $\Phi = (\phi_1, \phi_2, \dots, \phi_{N_\Gamma^r})^\top \in \mathbb{R}^{N_\Gamma \times N_\Gamma^r}$ represents the basis functions of the reduced space, N_Γ^r is the dimensionality of the reduced space, the vector $\boldsymbol{\beta} \in \mathbb{R}^{N_\Gamma^r}$ is the generalized coordinates of \mathbf{g} within the reduced space, which are to be determined.

We follow the approach presented in [28, 29] to define the basis functions ϕ_j as eigenfunctions of the Laplace-Beltrami operator on the interface Γ . Specifically, these eigenfunctions satisfy

$$-\Delta \phi_j = \mu_j \phi_j, \quad (22)$$

where μ_j denotes the eigenvalue corresponding to the eigenfunction ϕ_j . The advantages of using eigenfunctions of Laplace-Beltrami operator are detailed in [28]. For the problems considered in this work, where the interface is one-dimensional, the eigenfunctions ϕ_j reduce to a set of trigonometric functions [29], given by

$$\phi_j \in \left\{ 1, \dots, \cos\left(\frac{(N^r - 1)\pi}{L} \xi\right), \sin\left(\frac{\pi}{L} \xi\right), \dots, \sin\left(\frac{(N^r - 1)\pi}{L} \xi\right) \right\},$$

where ξ is a curvilinear coordinate defined on the interface and L the total length of the interface, N^r is the number of retained trigonometric functions. Note that $N_\Gamma^r = 2N^r - 1$.

By substituting the reduced representation of the control \mathbf{g} (as given in equation (21)) into the objective function (19) and the linearized constraints (20), we reformulate the optimization problem to solve for $(\mathbf{T}_f, \mathbf{T}_s, \boldsymbol{\beta})$. To address this optimization problem, as outlined in the previous section, we first derive the relationship between \mathbf{T}_f , \mathbf{T}_s and $\boldsymbol{\beta}$ from the linearized constraints. These relations are then substituted into the objective function to formulate a least-squares problem for the generalized coordinates $\boldsymbol{\beta}$ at each SQP iteration. We remark that to express \mathbf{T}_f , \mathbf{T}_s as function of $\boldsymbol{\beta}$, we now need to compute $(\mathbf{J}_f^{n+1,k})^{-1} (\mathbf{E}_f \Phi)$ and $(\mathbf{J}_s^{n+1,k})^{-1} (\mathbf{E}_s \Phi)$, which is significantly more efficient compared to the full computation when $N_\Gamma^r \ll N_\Gamma$. Hereafter, we refer to this approach as the reduced optimization-based method.

3.3 Optimization-based method for conjugate heat transfer problems

In Algorithm 1, we outline the extension of the optimization-based method for solving CHT problems. The algorithm demonstrates the procedure for a single time step, with line 2 representing the SQP iteration loop, where k denotes the SQP iteration number. The integration of the fluid solver into the SQP loop is achieved in line 3. This step ensures the velocity field from the fluid domain is updated iteratively to account for the interaction between fluid dynamics and heat transfer. Note that if we assume the fluid velocity is known (i.e., line 3 is removed), Algorithm 1 reduces to the SQP method for heat transfer problems alone, as described in Section 3.2.1, where only the heat transfer problem is iteratively solved.

Algorithm 1 optimization-based algorithm for CHT problems.

- 1: Initialize $\mathbf{T}_f^{n+1,0}$, $\mathbf{g}^{n+1,0}$.
 - 2: **for** $k = 0, \dots, K$ **do**
 - 3: Solve the fluid flow equations (1)-(2) using the temperature field $\mathbf{T}_f^{n+1,k}$ in the buoyancy term.
 This step yields the velocity field $\mathbf{u}_f^{n+1,k}$.
 - 4: Solve the optimization problem (19)-(20) for the heat transfer problem
 using $\mathbf{u}_f = \mathbf{u}_f^{n+1,k}$ for the convective term in the fluid heat equation.
 This step provides updated values for $\mathbf{T}_f^{n+1,k+1}$, $\mathbf{T}_s^{n+1,k+1}$, and $\mathbf{g}^{n+1,k+1}$.
 - 5: Terminate if the convergence criterion $\frac{\|\mathbf{g}^{n+1,k+1} - \mathbf{g}^{n+1,k}\|}{\|\mathbf{g}^{n+1,k}\|} < \text{tol}$ is satisfied.
 - 6: Update the variables as follows: $\mathbf{T}_f^{n+1,k} \leftarrow \mathbf{T}_f^{n+1,k+1}$, $\mathbf{T}_s^{n+1,k} \leftarrow \mathbf{T}_s^{n+1,k+1}$, $\mathbf{g}^{n+1,k} \leftarrow \mathbf{g}^{n+1,k+1}$.
 - 7: **end for**
-

Remark 3.2. *The optimization-based method is highly versatile and can be combined with any fluid solver, such as the SIMPLE method. To adapt the algorithm to a specific solver, it is sufficient to replace the step in line 3 with the corresponding method for solving the fluid flow.*

4 Numerical results

We present numerical results obtained using the semi-implicit method and the optimization-based method to illustrate overall numerical properties. The lid-driven cavity case illustrate the performance of the semi-implicit method; while the diffusion problem show the effectiveness of the OB method. Additionally, two CHT problems are simulated to further evaluate the methods. All numerical simulations are performed in MATLAB_R2024a on a commodity Laptop.

4.1 Lid-driven cavity

We apply the semi-implicit method to simulate laminar, incompressible flow in a square cavity with a side length of $L = 1$ [34, 22]. The left, right, and bottom boundaries are treated as no-slip walls, while the upper boundary is a moving top lid with a horizontal velocity of $u_0 = 1$. We vary the fluid viscosity μ to investigate flow behavior at different Reynolds numbers, $\text{Re} = \frac{\rho u_0 L}{\mu} = 100, 400, 1000$, with a fluid density of $\rho = 1$. Structured grids with $N \times N$ cells are used, where $N = 40$ for $\text{Re} = 100$ and $N = 120$ for $\text{Re} = 400$ and $\text{Re} = 1000$. The time step is set to $\Delta t = \text{CFL} \frac{\Delta x}{u_0}$, with a CFL number of 0.5, where Δx represents the characteristic mesh size. For this test case, no iterations are performed at each time step in the semi-implicit method (i.e., we set $K = 0$ for the iterative solver described in B). In Figure 3, we present the x -velocity field and the streamline pattern obtained at steady state using both the semi-implicit and SIMPLE methods for $\text{Re} = 1000$. Both methods yield comparable results. The steady state is achieved when the difference between two successive velocity fields is less than 10^{-5} :

$$\text{err} = \frac{\sqrt{\sum_{i=1}^{\text{Ncell}} |\mathbf{u}_i^{n+1} - \mathbf{u}_i^n|^2}}{\sqrt{\sum_{i=1}^{\text{Ncell}} |\mathbf{u}_i^{n+1}|^2}} < 10^{-5}. \quad (23)$$

In Figure 4, we present the velocity profile along the vertical line passing through the center of the cavity for different Reynolds numbers, compared to the reference results from [34]. The results show good agreement with the reference data. In Figure 5, we compare the time evolution of the velocity at the center point, using both the semi-implicit and SIMPLE methods. The results from both methods align well with each other. During the initial stages of the simulation, the SIMPLE method requires approximately 10 iterations per time step to converge, whereas the semi-implicit method, which does not rely on an iterative procedure for this test case, demonstrates superior computational efficiency. Despite the absence of an iterative procedure, the semi-implicit is still able to capture accurately the unsteady behavior of the flow.

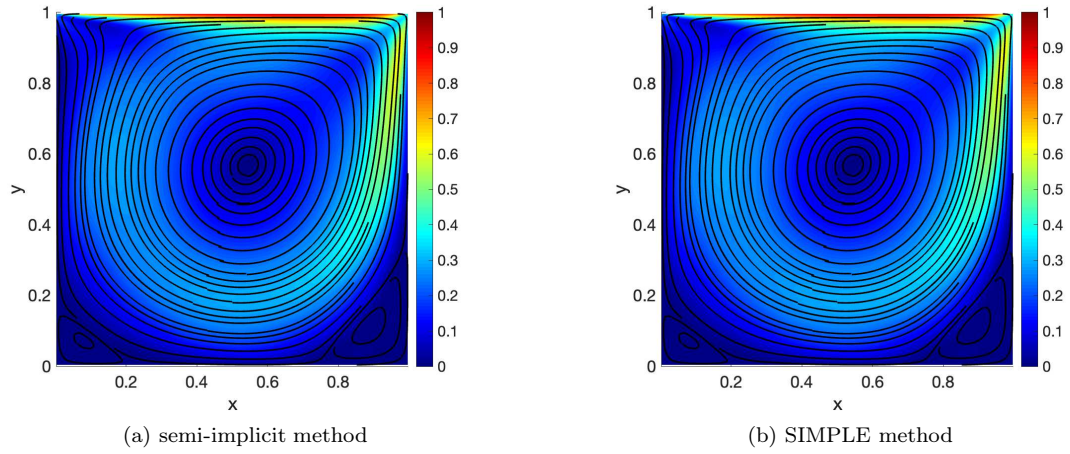


Figure 3: lid-driven cavity: x -velocity field and streamline pattern for $Re = 1000$.

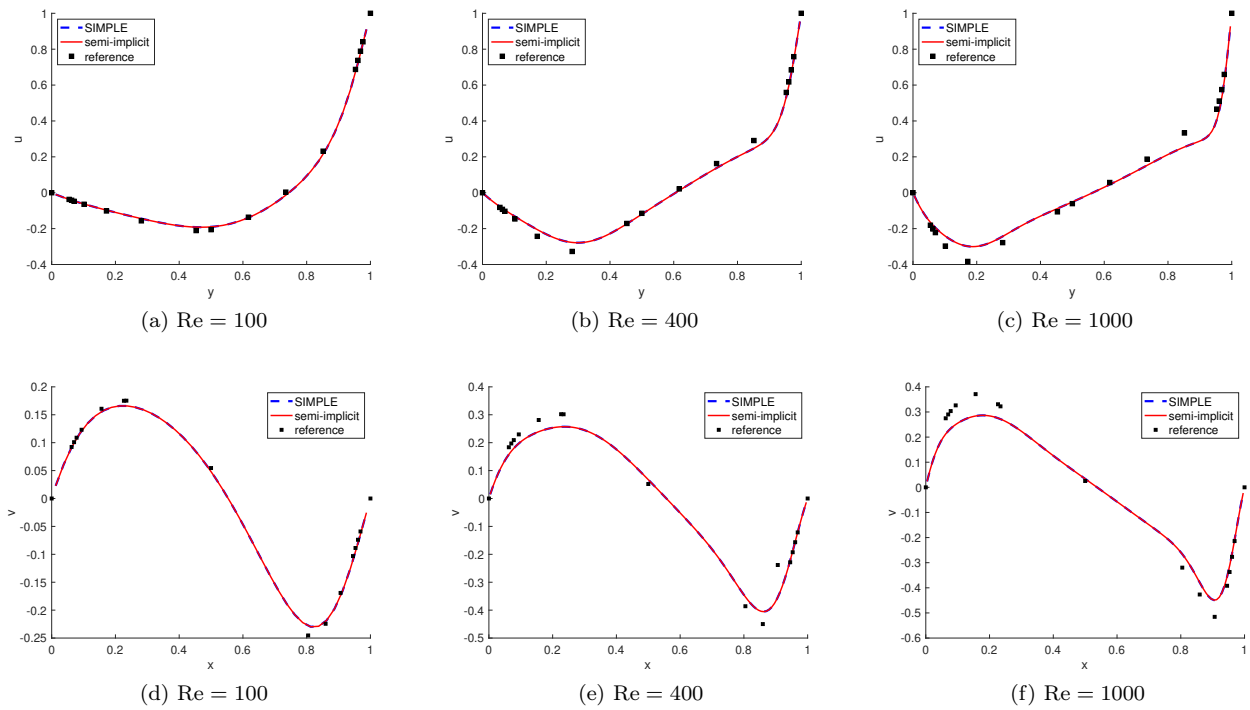


Figure 4: lid-driven cavity: (a), (b), (c) x -velocity along vertical line through geometric center of cavity; (d), (e), (f) y -velocity along horizontal line through geometric center of cavity.

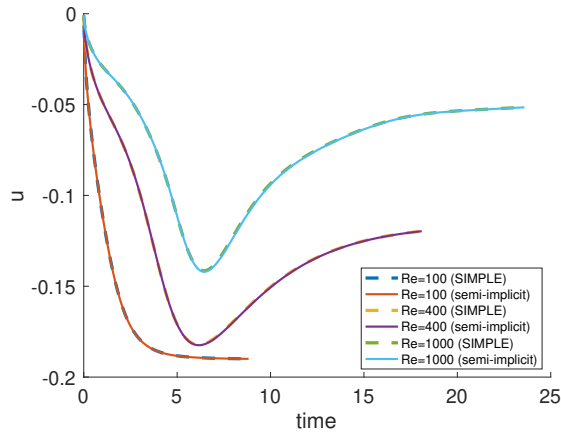


Figure 5: lid-driven cavity: evolution of the x -velocity at the center point.

4.2 Diffusion problem

We consider a steady-state diffusion problem governed by the equation

$$-\nabla \cdot (k \nabla T) = Q$$

in the domain $\Omega = (0, 1) \times (0, 2)$, with the analytical solution

$$T = 20 + x^2 - xy - 3y^2.$$

We examine three distinct cases based on varying thermal conductivities, as follows:

case 1: $k = 2T^3 - 0.1T^2 + T$,

case 2: $k = -0.1T^2 + T$,

case 3: $k = 1$.

For each case, the source term Q is computed to ensure that the diffusion equation is satisfied.

The computational domain is partitioned into two subdomains: a fluid domain and a solid domain, with the interface $\Gamma = (0, 1) \times \{1\}$. In both subdomains, the same diffusion equation is solved using the Dirichlet-to-Neumann (DtN) method and the OB method, with the appropriate coupling conditions as specified in equation (5) for the fluid-solid interface. Dirichlet boundary conditions are applied to the remaining boundaries. The convergence tolerance for both methods is set to 10^{-6} , and for the DtN method, a relaxation parameter of 0.2 is employed. For each case, three spatial discretizations are considered, with characteristic cell sizes $h = \frac{1}{20}, \frac{1}{40}, \frac{1}{80}$. The numerical results for **case 2** with $h = \frac{1}{80}$ are shown in Figure 6, where both the DtN and OB methods yield comparable results, with a maximum pointwise error of $\mathcal{O}(10^{-3})$ relative to the exact solution. A line at $y = 1$ is drawn to highlight the fluid-solid interface. Additionally, the test case is computed using the reduced OB method (cf. Section 3.2.2) with $N_r = 5$. The difference between the OB method with and without interface reduction is presented in Figure 6(d), where the difference is found to be of $\mathcal{O}(10^{-6})$.

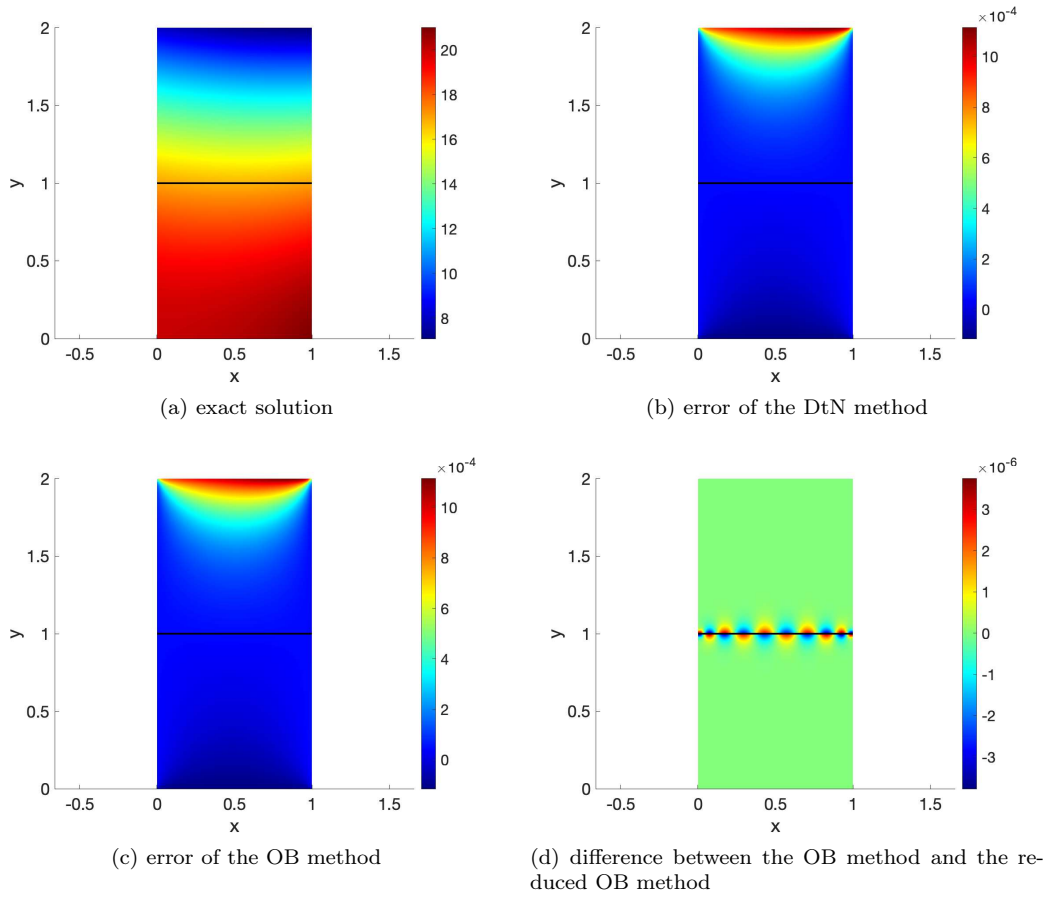


Figure 6: diffusion problem: **case 2**, $h = \frac{1}{80}$.

In Table 1, we compare the DtN method and the OB method in terms of the number of iterations and computational cost. We remark that the DtN method fails to converge for **case 1**, even with a relaxation parameter of 0.01. For all numerical cases, the OB method demonstrates superior performance compared to the DtN method. Additionally, the numerical simulation can be further accelerated using the reduced OB approach, with the acceleration becoming more significant as the spatial discretization is refined. We emphasize that the current code implementation is not optimized, with matrix assembly accounting for a large portion of the computational time. With a more efficient implementation, the reduced OB method should be more effective compared to the OB method. This work serves as a proof of concept, and thus, code optimization is not the primary focus.

	DtN method		OB method		reduced OB method	
	number iters	comp cost [s]	number iters	comp cost [s]	number iters	comp cost [s]
case 1 ($h = \frac{1}{20}$)	-	-	25	0.17	25	0.16
case 1 ($h = \frac{1}{40}$)	-	-	26	0.94	27	0.72
case 1 ($h = \frac{1}{80}$)	-	-	27	5.91	27	4.43
case 2 ($h = \frac{1}{20}$)	34	0.20	15	0.10	15	0.08
case 2 ($h = \frac{1}{40}$)	34	0.83	16	0.50	16	0.42
case 2 ($h = \frac{1}{80}$)	34	5.16	16	3.40	16	2.62
case 3 ($h = \frac{1}{20}$)	32	0.18	1	0.01	1	0.01
case 3 ($h = \frac{1}{40}$)	32	0.78	1	0.06	1	0.05
case 3 ($h = \frac{1}{80}$)	32	4.82	1	0.38	1	0.32

Table 1: comparison of the DtN and the OB methods in terms of number of iterations and computational cost.

4.3 Flow over a heated plate

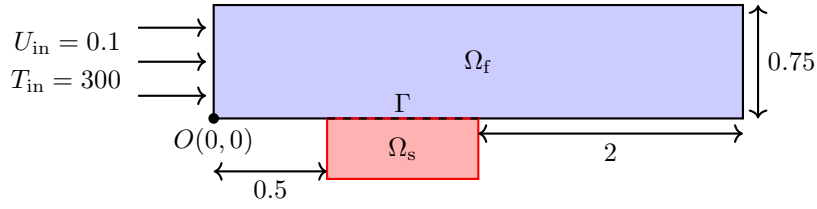


Figure 7: flow over a heated plate: illustration of the computational domain (not scaled).

In this test case, we simulate fluid flow over a heated plate [35, 36] and investigate the heat transfer characteristics resulting from convection in the fluid and conduction within the solid plate. The computational domain is depicted in Figure 7, with the geometric properties specified. The length of the plate, denoted as Ω_s , is $L = 1$, and the height of the plate is $b = L/4$.

The fluid enters from the left with a free-stream velocity of $U_{\text{in}} = 0.1$. The boundary conditions for the fluid flow are as follows: an outlet condition is specified on the right boundary; a Neumann condition is imposed on the top boundary; a slip wall condition is enforced to the bottom boundary upstream of the leading edge of the plate [35]; and a no-slip wall condition is applied to the remaining portion of the bottom boundary. For heat transfer in the fluid domain, a uniform temperature of $T_{\text{in}} = 300$ is imposed at the inlet. All boundaries, except for the interface where the coupling conditions in (5) are enforced, are treated as adiabatic, i.e., $\frac{\partial T}{\partial \mathbf{n}} = 0$. Regarding heat transfer in the solid plate, the bottom surface is maintained at a uniform temperature of $T_0 = 310$, while the left and right sides are assumed to be adiabatic.

The densities of both the fluid and the solid are taken to be equal, with $\rho_f = \rho_s = 1$. The dynamic viscosity of the fluid is chosen to be $\mu_f = 2 \times 10^{-4}$, which results in a Reynolds number $\text{Re} = \frac{\rho_f U_{\text{in}} L}{\mu_f} = 500$, based on the characteristic length of the plate L . The thermal properties of the solid plate include a thermal conductivity of $k_s = 100$ and a specific heat capacity of $c_{\text{ps}} = 100$. For the fluid, the thermal conductivity k_f and the specific heat capacity c_{pf} are computed using the conductivity ratio $k = \frac{k_s}{k_f}$ and the Prandtl number $\text{Pr} = \frac{\mu_f c_{\text{pf}}}{k_f}$. The effects of these parameters are investigated by varying the conductivity ratio, $k = 1, 2, 5, 20$, and the Prandtl number, $\text{Pr} = 0.01, 100$.

Note that gravity is not considered in this case, resulting in the decoupling of the energy equation from the mass and momentum equations of the fluid. As a consequence, the fluid flow \mathbf{u}_f can be determined by solving a purely fluid dynamics problem (1)-(2). Subsequently, the heat transfer problem can be addressed by solving the governing equations (3) and (4), with \mathbf{u}_f already known.

The fluid flow is solved using both the SIMPLE method and the proposed semi-implicit method. The resulting velocity fields in the x -direction are presented for both methods at steady-state conditions in Figure 8. The steady state is considered to be achieved when the relative change in velocity between two successive time steps is less than 10^{-5} (cf. equation (23)). We compare the evolution of x -direction velocity at a probe point $(0.5, 0.002)$, located near the leading edge of the solid plate, obtained using both the SIMPLE and semi-implicit methods in Figure 9. The results from both methods exhibit good agreement. The SIMPLE method requires 4 – 5 iterations per time step during the initial stages and 2 – 3 iterations when approaching steady state. In contrast, the semi-implicit method, which does not require iterations (i.e., we set $K = 0$ for the iterative solver described in B), demonstrates higher efficiency.

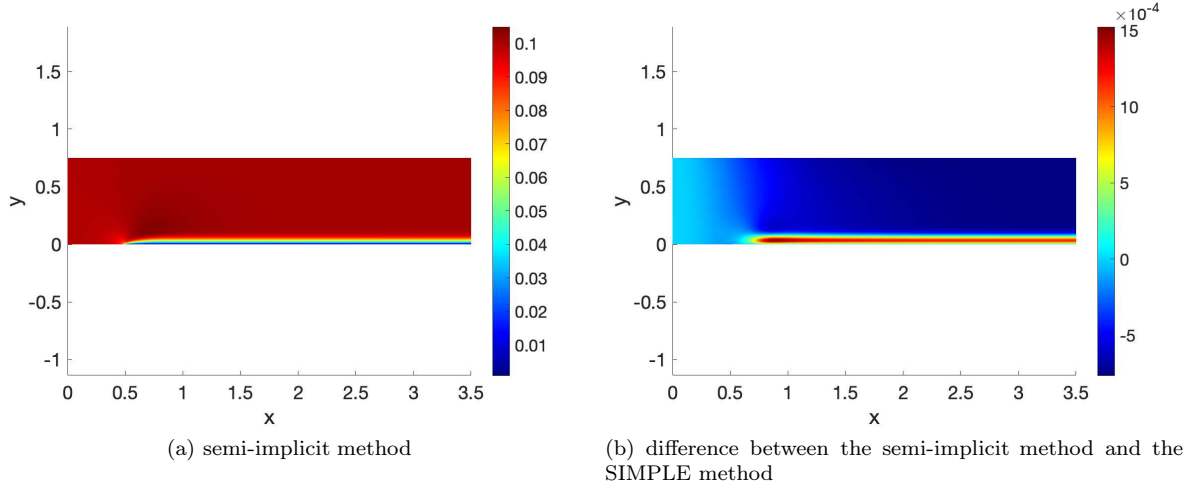


Figure 8: flow over a heated plate: x -velocity field at steady state.

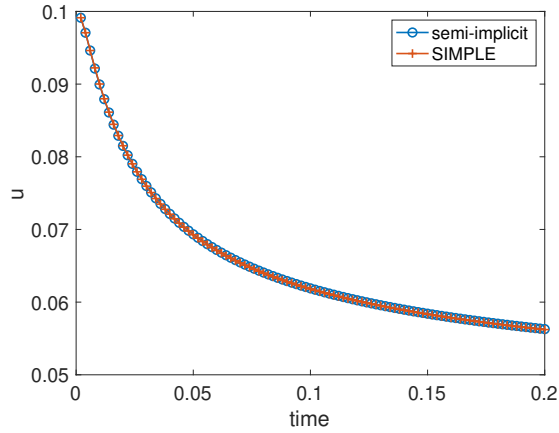


Figure 9: flow over a heated plate: evolution of the velocity at a probe point.

Once the fluid flow is solved using either the semi-implicit method or the SIMPLE method, the heat transfer between the fluid and the solid plate can subsequently be addressed using either the DtN method or the OB method. In Figure 10, we present the relative temperature distribution along the fluid-solid interface for both the DtN and OB methods, compared against the reference results provided in [35] for various conductivity ratios k and Prandtl numbers Pr , where the relative temperature is defined as:

$$T_{\text{rel}} = \frac{T - T_{\text{in}}}{T_0 - T_{\text{in}}}.$$

Both methods yield results in close agreement with each other and the reference values. In this test case, as the heat transfer model is linear, the OB method converges within a single iteration, similar to **case 3** in the diffusion problem discussed in Section 4.2. For the case with $Pr = 0.01$, we use a relaxation parameter of 0.2 for the DtN method, which requires approximately 35–65 iterations to attain convergence, for different choices of k . The OB method achieves a speed-up factor of 12–22 compared to the DtN method, highlighting its superior efficiency. For the case with $Pr = 100$, the efficiency of the OB method is even more pronounced, as the DtN method exhibits convergence difficulties, requiring a significantly reduced relaxation parameter of 0.05 to ensure convergence.

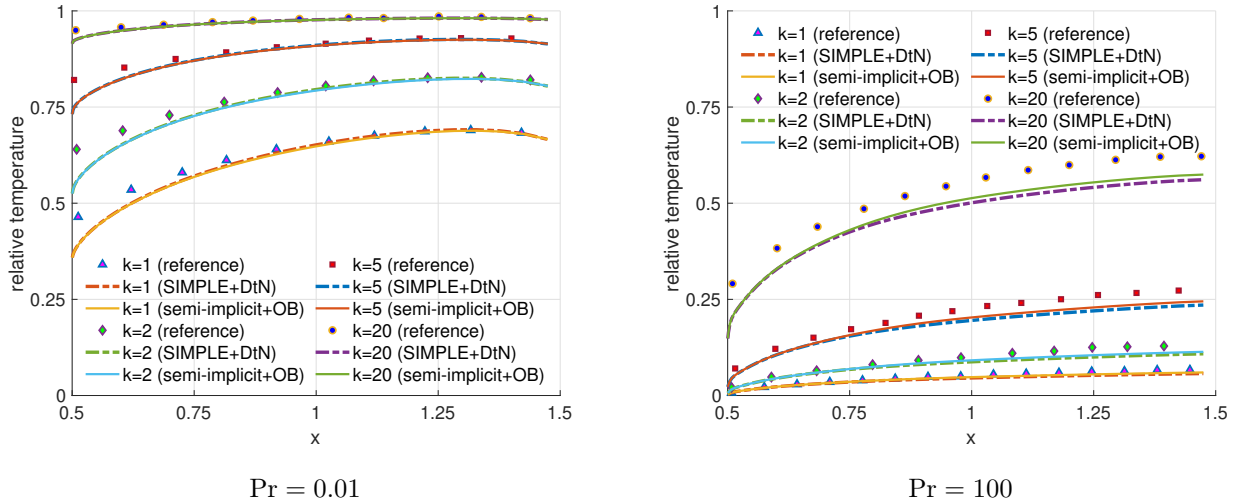


Figure 10: flow over a heated plate: relative temperature distribution along the fluid-solid interface for various values of k and Pr .

4.4 Natural convection

We consider natural convection in a square enclosure Ω_f , as illustrated in Figure 1, with a length of $L = 1$. The right side is heated by a solid domain Ω_s of width $b = 0.2$. Since the buoyancy term is included, Algorithm 1 is applied to solve this problem. For the fluid domain, a no-slip wall condition is imposed for the fluid flow. The top and bottom boundaries are considered adiabatic, while the left boundary is maintained at a cold temperature $T_c = 1$. In the solid domain, the top and bottom boundaries are also adiabatic, whereas the right boundary is set to a hot temperature $T_h = 2$. The gravitational acceleration is given by $\mathbf{g}_0 = (0, -1)^\top$, and the reference temperature in the buoyancy term is chosen as $T_{\text{ref}} = T_c$.

We consider three parameter settings [14, 16, 8]:

case 1: $\rho_f = 1$, $\mu_f = 0.7$, $\beta = 0.7 \times 10^5$, $\rho_s = 7.5 \times 10^3$, $k_s = 1.6 \times 10^3$, $c_{ps} = 0.5$, $k = 1.6 \times 10^3$, $Pr = 0.7$.

case 2: $\rho_f = 1$, $\mu_f = 7$, $\beta = 4.9 \times 10^5$, $\rho_s = 7.5$, $k_s = 80$, $c_{ps} = 0.12$, $k = 80$, $Pr = 7$.

case 3: $\rho_f = 1$, $\mu_f = 7$, $\beta = 4.9 \times 10^5$, $\rho_s = 7.5$, $k_s = 2.7$, $c_{ps} = 0.0576$, $k = 2.7$, $Pr = 7$.

The Prandtl number is given by $Pr = \frac{\mu_f c_{pf}}{k_f}$. These three test cases correspond to an increasing ratio of the thermal effusivities of the coupled domains, defined as

$$\sigma = \frac{k_f}{k_s} \sqrt{\frac{\alpha_s}{\alpha_f}},$$

where the thermal diffusivity is defined as $\alpha_{(\cdot)} = \frac{k_{(\cdot)}}{\rho_{(\cdot)} c_{p(\cdot)}}$, $(\cdot) = f, s$. The thermal effusivity ratios are $\sigma = 3.95 \times 10^{-4}$, 0.12, and 0.93, respectively, indicating weak thermal interaction between the fluid and solid domains in **case 1**, strong interaction in **case 3**, and an intermediate level of interaction in **case 2**.

For this test case, we rely on the iterative semi-implicit method, as outlined in Algorithm 2, to solve the fluid flow. We use a spatial discretization of size $\Delta x = \Delta y = \frac{1}{80}$, and a time step of $\Delta t = 0.001$. The number of iterations is slightly smaller than that required by the SIMPLE method. However, a key advantage is that the same matrix is solved at each iteration and time step. The outer loop of the optimization-based algorithm (cf. Algorithm 1) typically requires 5 iterations to converge in the initial stages and 2 iterations as it approaches the steady state. Since the heat transfer problem is linear in this test case, the inner optimization problem converges within 1 sub-iteration. In contrast, if we use the DtN method instead of the OB method in step 4 of Algorithm 1, the DtN method typically requires 20–40 sub-iterations. These results demonstrate the improved efficiency of the proposed approach.

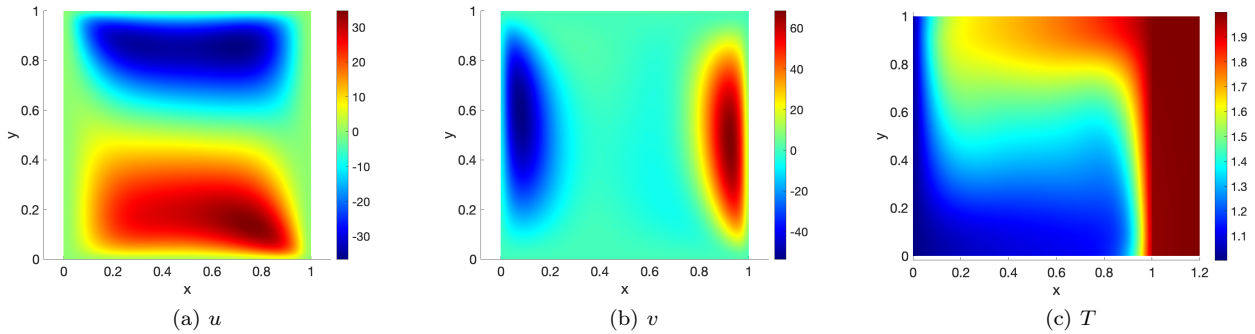


Figure 11: natural convection problem: **case 2**, solution fields at $t = 0.07$.

We present the solution fields at $t = 0.07$ for **case 2** in Figure 11. As observed, the fluid circulates in the counter-clockwise direction. The flow moves upward along the hot fluid-solid interface, leading to an increase in temperature in the y -direction at the interface. Similarly, the flow moves downward along the cold left boundary, causing a temperature decrease in the negative y -direction at the left boundary. Similar behavior is observed in the other two cases. We present the dimensionless temperature profile θ in Figure 12 for the three test cases, defined as

$$\theta = \frac{T - T_c}{T_h - T_c}.$$

Specifically, Figure 12(a) shows the temperature profile along $y = 0.5$ at $t = 0.07$. The obtained results exhibit good agreement with the reference data [8]. In Figure 12(b), we present the time evolution of the temperature at the center of the fluid domain, located at $(0.5, 0.5)$. The proposed approach accurately captures the dynamic behavior.

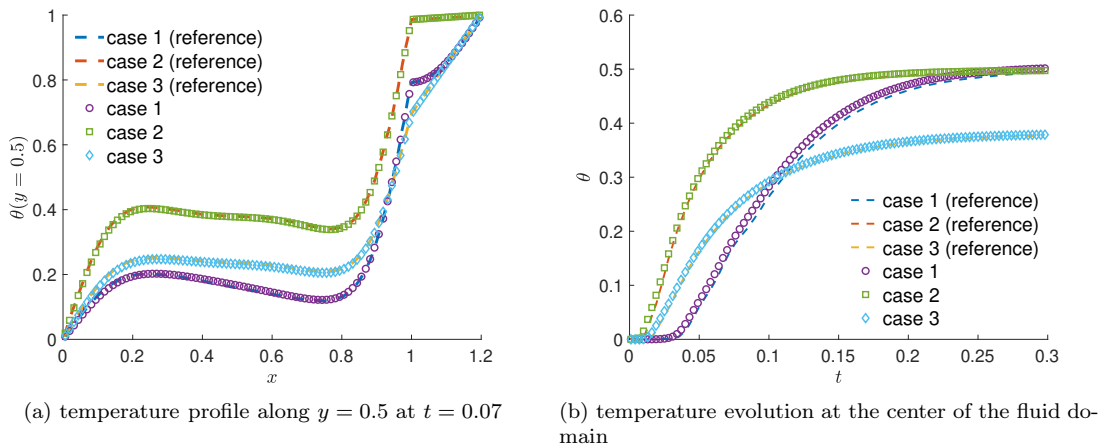


Figure 12: natural convection problem: temperature profile.

5 Conclusions

We proposed a partitioned numerical framework for solving conjugate heat transfer problems by integrating a semi-implicit method for fluid flow with an optimization-based approach for heat transfer across the fluid-solid interface. The semi-implicit method efficiently solves the incompressible Navier-Stokes equations while maintaining stability under a Courant-Friedrichs-Lewy (CFL) condition, with stability condition rigorously established through von Neumann analysis. The optimization-based method effectively enforces fluid-solid interface conditions and efficiently solves heat transfer between the fluid and solid domains. The framework improves computational performance by eliminating sub-iterations within each time step for solving the Navier-Stokes equations and by leveraging a sequential quadratic programming approach to solve the constrained optimization problem. Numerical results validate the proposed method, showing improved efficiency compared to the SIMPLE method for fluid flow and the Dirichlet-to-Neumann method for heat transfer.

In the future, we plan to develop efficient factorization techniques for solving the semi-implicit system to enhance computational efficiency; we plan to extend the method towards a nearly implicit scheme [37], enabling for large time steps and steady-state computations. Additionally, the optimization-based method will

be applied to more challenging problems, such as those involving complex geometries or highly nonlinear thermal interactions, to assess its robustness in real-world engineering applications. Furthermore, the introduction of Robin-type boundary conditions in the optimization-based formulation will be explored to improve interface coupling and accelerate convergence in partitioned solvers.

Acknowledgements

The work of Xiandong Liu and Lei Zhang is supported by the Fundamental Research Funds for the Central Universities of Tongji University, and National Natural Science Foundation of China (grant number: 12301557). The work of Liang Fang and Lei Zhang is supported by the Interdisciplinary Joint Research Project of Tongji University.

A Numerical stability

We derive the stability condition of the proposed semi-implicit method presented in 3.1. Following the approach in [38], we consider the non-dimensional form of the governing equations and introduce an artificial compressibility term into the mass conservation equation. Additionally, to facilitate analysis, we include a convective term in the mass conservation equation, thereby reformulating the mass conservation equation into a form analogous to that of compressible flows. The stability properties are examined using von Neumann stability analysis applied to a two-dimensional problem on structured grids.

With the non-dimensional formulation, the introduction of the artificial compressibility term, and the inclusion of the convective term, the Navier-Stokes equations considered in this analysis are given as

$$\frac{\partial \rho}{\partial t} + \rho \frac{\partial u}{\partial x} + \rho \frac{\partial v}{\partial y} + u \frac{\partial \rho}{\partial x} + v \frac{\partial \rho}{\partial y} = 0, \quad (24)$$

$$\frac{\partial u}{\partial t} + u \frac{\partial u}{\partial x} + v \frac{\partial u}{\partial y} - \mu \left(\frac{\partial^2 u}{\partial x^2} + \frac{\partial^2 u}{\partial y^2} \right) + \frac{\partial p}{\partial x} = 0, \quad (25)$$

$$\frac{\partial v}{\partial t} + v \frac{\partial v}{\partial y} + u \frac{\partial v}{\partial x} - \mu \left(\frac{\partial^2 v}{\partial x^2} + \frac{\partial^2 v}{\partial y^2} \right) + \frac{\partial p}{\partial y} = 0, \quad (26)$$

where the artificial density ρ is related to the dimensionless pressure through the artificial speed of sound c as

$$\rho = \frac{p}{c^2}.$$

Assuming the velocity components satisfy $u > 0$ and $v > 0$, we apply the semi-implicit to the above system (24)-(26). By linearizing the system around a reference state $(p_0, u_0, v_0, \rho_0, c_0)$, we obtain the following discretized equations

$$\begin{aligned} p_{j,k}^{n+1} - p_{j,k}^n + \frac{\rho_0 c_0^2 \Delta t}{\Delta x} \left(u_{j+\frac{1}{2},k}^{n+1} - u_{j-\frac{1}{2},k}^{n+1} \right) + \frac{\rho_0 c_0^2 \Delta t}{\Delta y} \left(v_{j,k+\frac{1}{2}}^{n+1} - v_{j,k-\frac{1}{2}}^{n+1} \right) \\ + \frac{u_0 \Delta t}{\Delta x} (p_{j,k}^n - p_{j-1,k}^n) + \frac{v_0 \Delta t}{\Delta y} (p_{j,k}^n - p_{j,k-1}^n) = 0, \end{aligned} \quad (27)$$

$$\begin{aligned} u_{j,k}^{n+1} - u_{j,k}^n + \frac{u_0 \Delta t}{\Delta x} (u_{j,k}^n - u_{j-1,k}^n) + \frac{v_0 \Delta t}{\Delta y} (u_{j,k}^n - u_{j,k-1}^n) \\ - \frac{2\mu \Delta t}{(\Delta x)^2} \frac{u_{j+1,k}^{n+1} - 2u_{j,k}^{n+1} + u_{j-1,k}^{n+1}}{2} - \frac{2\mu \Delta t}{(\Delta y)^2} \frac{u_{j,k+1}^{n+1} - 2u_{j,k}^{n+1} + u_{j,k-1}^{n+1}}{2} + \frac{\Delta t}{2\Delta x} (p_{j+1,k}^{n+1} - p_{j-1,k}^{n+1}) = 0, \end{aligned} \quad (28)$$

$$\begin{aligned} v_{j,k}^{n+1} - v_{j,k}^n + \frac{v_0 \Delta t}{\Delta y} (v_{j,k}^n - v_{j,k-1}^n) + \frac{u_0 \Delta t}{\Delta x} (v_{j,k}^n - v_{j-1,k}^n) \\ - \frac{2\mu \Delta t}{(\Delta x)^2} \frac{v_{j+1,k}^{n+1} - 2v_{j,k}^{n+1} + v_{j-1,k}^{n+1}}{2} - \frac{2\mu \Delta t}{(\Delta y)^2} \frac{v_{j,k+1}^{n+1} - 2v_{j,k}^{n+1} + v_{j,k-1}^{n+1}}{2} + \frac{\Delta t}{2\Delta y} (p_{j,k+1}^{n+1} - p_{j,k-1}^{n+1}) = 0. \end{aligned} \quad (29)$$

Moreover, the Rhie-Chow interpolation is employed to compute the velocity at cell face in the mass equation (27)

$$u_{j+\frac{1}{2},k}^{n+1} = \frac{1}{2}(u_{j,k}^{n+1} + u_{j+1,k}^{n+1}) - \frac{\Delta t}{(1+C_\mu)} \frac{p_{j+1,k}^{n+1} - p_{j,k}^{n+1}}{\Delta x} + \frac{\Delta t}{2(1+C_\mu)} \left(\frac{p_{j+1,k}^{n+1} - p_{j-1,k}^{n+1}}{2\Delta x} + \frac{p_{j+2,k}^{n+1} - p_{j,k}^{n+1}}{2\Delta x} \right), \quad (30)$$

$$v_{j,k+\frac{1}{2}}^{n+1} = \frac{1}{2}(v_{j,k}^{n+1} + v_{j,k+1}^{n+1}) - \frac{\Delta t}{(1+C_\mu)} \frac{p_{j,k+1}^{n+1} - p_{j,k}^{n+1}}{\Delta y} + \frac{\Delta t}{2(1+C_\mu)} \left(\frac{p_{j,k+1}^{n+1} - p_{j,k-1}^{n+1}}{2\Delta y} + \frac{p_{j,k+2}^{n+1} - p_{j,k}^{n+1}}{2\Delta y} \right), \quad (31)$$

where $C_\mu = \frac{2\mu\Delta t}{(\Delta x)^2} + \frac{2\mu\Delta t}{(\Delta y)^2}$.

A von Neumann analysis can be performed by substituting $\phi_{j,k}^n$ with $\phi e^{-ij\theta_1} e^{-ik\theta_2} g^n$, where g represents the eigenvalue of the amplification matrix. This leads to the following system of equations

$$\begin{aligned} p [g - 1 + C_{m1}k_{11} + C_{m2}k_{12} + (\rho_0 C_{s1}^2 C_{\mu3} k_{31} + \rho_0 C_{s2}^2 C_{\mu3} k_{32}) g] + u(\rho_0 c_0 C_{s1} k_{21}) g + v(\rho_0 c_0 C_{s2} k_{22}) g &= 0, \\ p (c_0^{-1} C_{s1} k_{21}) g + u [g - 1 + C_{m1}k_{11} + C_{m2}k_{12} - (C_{\mu1}k_{41} + C_{\mu2}k_{42}) g] &= 0, \\ p (c_0^{-1} C_{s2} k_{22}) g + v [g - 1 + C_{m2}k_{12} + C_{m1}k_{11} - (C_{\mu1}k_{41} + C_{\mu2}k_{42}) g] &= 0, \end{aligned}$$

where

$$\begin{aligned} C_{m1} &= \frac{u_0\Delta t}{\Delta x}, \quad C_{m2} = \frac{v_0\Delta t}{\Delta y}, \quad C_{s1} = \frac{c_0\Delta t}{\Delta x}, \quad C_{s2} = \frac{c_0\Delta t}{\Delta y}, \quad C_{\mu1} = \frac{2\mu\Delta t}{(\Delta x)^2}, \quad C_{\mu2} = \frac{2\mu\Delta t}{(\Delta y)^2}, \quad C_{\mu3} = \frac{1}{1 + C_\mu}, \\ k_{1l} &= 1 - e^{i\theta_l} = 1 - \cos\theta_l - i \sin\theta_l, \quad k_{2l} = \frac{e^{-i\theta_l} - e^{i\theta_l}}{2} = -i \sin\theta_l, \\ k_{3l} &= \frac{e^{2i\theta_l} - 4e^{i\theta_l} + 6 - 4e^{-i\theta_l} + e^{-2i\theta_l}}{4} = (\cos\theta_l - 1)^2, \quad k_{4l} = \frac{e^{-i\theta_l} - 2 + e^{i\theta_l}}{2} = \cos\theta_l - 1, \quad l = 1, 2. \end{aligned}$$

In matrix form, this system can be written as:

$$\begin{pmatrix} G_{11}(g) & g\rho_0 c_0 C_{s1} k_{21} & g\rho_0 c_0 C_{s2} k_{22} \\ g c_0^{-1} C_{s1} k_{21} & G_{22}(g) & 0 \\ g c_0^{-1} C_{s2} k_{22} & 0 & G_{22}(g) \end{pmatrix} \begin{pmatrix} p \\ u \\ v \end{pmatrix} = \begin{pmatrix} 0 \\ 0 \\ 0 \end{pmatrix},$$

where

$$\begin{aligned} G_{11}(g) &= g(1 + \rho_0 C_{s1}^2 C_{\mu3} k_{31} + \rho_0 C_{s2}^2 C_{\mu3} k_{32}) + G_k, \\ G_{22}(g) &= g(1 - C_{\mu1}k_{41} - C_{\mu2}k_{42}) + G_k, \\ G_k &= C_{m1}k_{11} + C_{m2}k_{12} - 1. \end{aligned}$$

The characteristic polynomial can be computed as:

$$\phi_3(g) = \phi_1(g)\phi_2(g), \tag{32}$$

where the subscripts of ϕ denote the degree of the polynomial and

$$\begin{aligned} \phi_1(g) &= G_{22}(g), \\ \phi_2(g) &= G_{22}(g)G_{11}(g) - g^2\rho_0 (C_{s1}^2 k_{21}^2 + C_{s2}^2 k_{22}^2). \end{aligned}$$

Based on the characteristic polynomial derived through von Neumann analysis, we now proceed with the proof of Theorem 1, established in Section 3.1, which states the stability condition for the semi-implicit method. To do so, we first introduce the following definitions and lemma [39].

Definition 1. A polynomial ϕ is a von Neumann polynomial if and only if all its roots r_v satisfy the condition:

$$|r_v| \leq 1.$$

Definition 2. A polynomial ϕ is a simple von Neumann polynomial if and only if ϕ is a von Neumann polynomial and its roots on the unit circle are simple roots.

Definition 3. For a polynomial ϕ of degree d , its conjugate polynomial ϕ^* is defined as:

$$\phi^*(g) = \sum_{l=0}^d \bar{a}_{d-l} g^l,$$

where \bar{a}_{d-l} denotes the conjugate of a_{d-l} , moreover we define

$$\phi_{d-1}(g) = \frac{\phi_d^*(0)\phi_d(g) - \phi_d(0)\phi_d^*(g)}{g}.$$

Lemma 2. ϕ_d is a simple von Neumann polynomial if and only if

- (1) $|\phi_d(0)| < |\phi_d^*(0)|$, and
- (2) ϕ_{d-1} is a simple von Neumann polynomial.

With these definitions and Lemma 2 established, we now proceed to prove Theorem 1.

Proof. It suffices to demonstrate that the roots of characteristic polynomial $\phi_3(g)$ (cf. equation (32)) satisfy $|g| \leq 1$ under the CFL condition (10). For the root of polynomial $\phi_1(g)$, denoted as g_1 , we have the following inequality

$$|g_1| = \frac{|G_k|}{|1 - C_{\mu 1} k_{41} - C_{\mu 2} k_{42}|} = \frac{|G_k|}{1 + C_{\mu 1}(1 - \cos \theta_1) + C_{\mu 2}(1 - \cos \theta_2)} \leq |G_k|. \quad (33)$$

The right side of this inequality can be shown to satisfy

$$|G_k| \leq 1, \quad (34)$$

provided that $C_m \in [0, 1]$, where $C_m = C_{m1} + C_{m2}$.

The proof will be complete once we establish that $\phi_2(g)$ is a simple von Neumann polynomial under the condition $C_m \in [0, 1]$. Let $\phi_2(g)$ be expressed as

$$\phi_2(g) = Ag^2 + Bg + C,$$

where the coefficients are defined as:

$$\begin{aligned} A &= (1 + \rho_0 C_{s1}^2 C_{\mu 3} k_{31} + \rho_0 C_{s2}^2 C_{\mu 3} k_{32}) (1 - C_{\mu 1} k_{41} - C_{\mu 2} k_{42}) - \rho_0 (C_{s1}^2 k_{21}^2 + C_{s2}^2 k_{22}^2) \\ &= (1 + D)(1 + E) + \rho_0 (C_{s1}^2 \sin^2 \theta_1 + C_{s2}^2 \sin^2 \theta_2) > 1, \\ B &= G_k (2 + \rho_0 C_{s1}^2 C_{\mu 3} k_{31} + \rho_0 C_{s2}^2 C_{\mu 3} k_{32} - C_{\mu 1} k_{41} - C_{\mu 2} k_{42}) \\ &= G_k (2 + D + E), \\ C &= G_k^2, \\ D &= \rho_0 C_{s1}^2 C_{\mu 3} (\cos \theta_1 - 1)^2 + \rho_0 C_{s2}^2 C_{\mu 3} (\cos \theta_2 - 1)^2, \\ E &= C_{\mu 1} (1 - \cos \theta_1) + C_{\mu 2} (1 - \cos \theta_2). \end{aligned}$$

The conjugate polynomial $\phi_2^*(g)$ is given by (cf. definition 3):

$$\phi_2^*(g) = \bar{C}g^2 + \bar{B}g + A. \quad (35)$$

Now, we apply the first condition in Lemma 2, which states that $|\phi_2(0)| < |\phi_2^*(0)|$. This implies

$$|C| < |A|. \quad (36)$$

From equation (34), we know that $|C| = |G_k^2| = |G_k|^2 \leq 1$. Additionally, since $A > 1$, the first condition of Lemma 2 is satisfied.

Next, we verify the second condition in Lemma 2, which requires:

$$|AB - \bar{B}C| \leq A^2 - |C|^2. \quad (37)$$

Since $\bar{B}C = B|C|$, this condition becomes

$$|B| \leq A + |C|. \quad (38)$$

Substituting the expressions for A, B, C , we obtain

$$|G_k|(2 + D + E) \leq (1 + D)(1 + E) + \rho_0 C_{s1}^2 \sin^2 \theta_1 + \rho_0 C_{s2}^2 \sin^2 \theta_2 + |G_k|^2.$$

This inequality can be verified using the following relations:

$$\begin{aligned} 2|G_k| &\leq 1 + |G_k|^2, \\ |G_k|(D + E) &\leq D + E, \\ 0 &\leq DE, \\ 0 &\leq \rho_0 C_{s1}^2 \sin^2 \theta_1 + \rho_0 C_{s2}^2 \sin^2 \theta_2. \end{aligned}$$

Thus, by Lemma 2, we conclude that $\phi_2(g)$ is a simple von Neumann polynomial under the condition $C_m \in [0, 1]$. □

B Iterative solver

We propose an iterative procedure to solve the global system (7)-(9), following the framework of the SIMPLE method. The approach consists of three main steps: first, the momentum equation is solved using the pressure from the previous subiteration to obtain a predicted velocity; next, a linear system for the pressure correction is derived from the mass conservation equation; finally, the velocity field is corrected based on the computed pressure correction. The detailed procedure is outlined in Algorithm 2.

Compared to the SIMPLE method, the proposed approach explicitly treats the nonlinear convective term, resulting in a linear system for the predicted velocity and another for the pressure correction that remain unchanged across subiterations and time steps. Consequently, these systems can be factorized in advance, significantly improving computational efficiency.

Algorithm 2 Iterative semi-implicit method

1: Initialize $(\mathbf{u}_f)_C^{n+1,0}, P_C^{n+1,0}$.

2: **for** $k = 0, \dots, K$ **do**

3: Compute the predicted velocity at cell center $(\mathbf{u}_f)_C^{n+1,k+\frac{1}{2}}$:

$$a_C(\mathbf{u}_f)_C^{n+1,k+\frac{1}{2}} + \sum_{F \in \text{nb}(C)} a_F(\mathbf{u}_f)_F^{n+1,k+\frac{1}{2}} = -\nabla P_C^{n+1,k} + \mathbf{B}_C^n.$$

4: Compute the predicted velocity at cell boundary based on the Rhie et Chow interpolation (cf. equation (9)):

$$(\mathbf{u}_f)_b^{n+1,k+\frac{1}{2}} = \frac{1}{2} \left[(\mathbf{u}_f)_C^{n+1,k+\frac{1}{2}} + (\mathbf{u}_f)_{C'}^{n+1,k+\frac{1}{2}} \right] - (\mathbf{D}_f)_b \left[(\nabla P)_b^{n+1,k} - \overline{(\nabla P)_b^{n+1,k}} \right].$$

5: Obtain the pressure correction P' by solving the mass equation

$$\sum_{b(C)} \left[(\mathbf{u}_f)_b^{n+1,k+\frac{1}{2}} + (\mathbf{u}_f)_b' \right] \cdot \mathbf{S}_{f,b} = 0,$$

where the velocity correction $(\mathbf{u}_f)_b'$ is related to the pressure correction P'_C by $(\mathbf{u}_f)_b' = -(\mathbf{D}_f)_b(\nabla P)_b'$.

6: Determine the corrected velocity and pressure as

$$\begin{aligned} (\mathbf{u}_f)_C^{n+1,k+1} &= (\mathbf{u}_f)_C^{n+1,k+\frac{1}{2}} - (\mathbf{D}_f)_C(\nabla P)_C', \\ P_C^{n+1,k+1} &= P_C^{n+1,k} + P'_C. \end{aligned}$$

7: Terminate if the convergence criterion $\frac{\|(\mathbf{u}_f)^{n+1,k+1} - (\mathbf{u}_f)^{n+1,k}\|}{\|(\mathbf{u}_f)^{n+1,k}\|} < \text{tol}$ is satisfied.

8: Update the variables as follows: $(\mathbf{u}_f)_C^{n+1,k} \leftarrow (\mathbf{u}_f)_C^{n+1,k+1}$, $P_C^{n+1,k} \leftarrow P_C^{n+1,k+1}$.

9: **end for**

Remark. In the previous algorithm, we can set $K = 0$, meaning that no iterative procedure is involved. In this case, it can be straightforwardly derived that the approach is equivalent to solving

$$\begin{aligned} \sum_{b(C)} (\mathbf{u}_f)_b^{n+1} \cdot \mathbf{S}_{f,b} &= 0, \\ a_C(\mathbf{u}_f)_C^{n+1} + \sum_{F \in \text{nb}(C)} a_F(\mathbf{u}_f)_F^{n+1,\frac{1}{2}} &= -\nabla P_C^{n+1} + \mathbf{B}_C^n, \\ (\mathbf{u}_f)_b^{n+1} &= \frac{1}{2} \left[(\mathbf{u}_f)_C^{n+1} + (\mathbf{u}_f)_{C'}^{n+1} \right] - (\mathbf{D}_f)_b \left[(\nabla P)_b^{n+1} - \overline{(\nabla P)_b^{n+1}} \right]. \end{aligned}$$

Specifically, the mass conservation equation and the Rhie-Chow interpolation remain unchanged, while the momentum equation is solved using the predicted velocity for the neighboring cells of cell C .

For certain scenarios, stable and reliable numerical results can still be obtained, provided that the CFL condition (cf. equation (10)) is satisfied. This approach offers efficiency advantages by reducing computational cost, as it eliminates the need for iterative corrections. In the numerical results, we explicitly indicate whether this semi-implicit method with $K = 0$ is applied.

References

- [1] C. Srinivasan, X. Yang, J. Schlautman, D. Wang, S. Gangaraj, Conjugate heat transfer CFD analysis of an oil cooled automotive electrical motor, *SAE International Journal of Advances and Current Practices in Mobility* 2 (2020-01-0168) (2020) 1741–1753. doi:10.4271/2020-01-0168.
- [2] R. Burke, C. Copeland, T. Duda, M. Reyes-Belmonte, Lumped capacitance and 3D CFD conjugate heat transfer modelling of an automotive turbocharger, in: *Turbo Expo: Power for Land, Sea, and Air*, Vol. 56796, American Society of Mechanical Engineers, 2015, p. V008T23A004.
- [3] W. Zhu, W. Lin, S. Zhang, S. Yang, T. Wu, R. Ma, T.-F. Cao, Y.-J. Dai, W.-Q. Tao, Modeling and analysis of fluid-solid coupling heat transfer and fluid flow in transonic nozzle, *Applied Thermal Engineering* 260 (2025) 124885. doi:10.1016/j.applthermaleng.2024.124885.
- [4] R. Sarma, P. K. Mondal, Entropy generation minimization in a pressure-driven microflow of viscoelastic fluid with slippage at the wall: effect of conjugate heat transfer, *Journal of Heat Transfer* 140 (5) (2018) 052402. doi:10.1115/1.4038451.
- [5] D. Deb, S. K. Mehta, S. Wongwises, P. K. Mondal, Augmented electronic cooling strategy: effect of foam pore size for forced convective flow through wavy canopy, *Microsystem Technologies* (2025) 1–12doi:10.1007/s00542-024-05841-6.
- [6] X. Chen, P. Han, A note on the solution of conjugate heat transfer problems using SIMPLE-like algorithms, *International Journal of Heat and Fluid Flow* 21 (4) (2000) 463–467. doi:10.1016/S0142-727X(00)00028-X.
- [7] X. Pan, K. Kim, C. Lee, J.-I. Choi, Fully decoupled monolithic projection method for natural convection problems, *Journal of Computational Physics* 334 (2017) 582–606. doi:10.1016/j.jcp.2017.01.022.
- [8] X. Pan, C. Lee, J.-I. Choi, Efficient monolithic projection method for time-dependent conjugate heat transfer problems, *Journal of Computational Physics* 369 (2018) 191–208. doi:10.1016/j.jcp.2018.05.010.
- [9] W. D. Henshaw, K. K. Chand, A composite grid solver for conjugate heat transfer in fluid–structure systems, *Journal of Computational Physics* 228 (10) (2009) 3708–3741. doi:10.1016/j.jcp.2009.02.007.
- [10] V. Kazemi-Kamyab, A. van Zuijlen, H. Bijl, Accuracy and stability analysis of a second-order time-accurate loosely coupled partitioned algorithm for transient conjugate heat transfer problems, *International Journal for Numerical Methods in Fluids* 74 (2) (2014) 113–133. doi:10.1002/flid.3842.
- [11] T. Verstraete, S. Scholl, Stability analysis of partitioned methods for predicting conjugate heat transfer, *International Journal of Heat and Mass Transfer* 101 (2016) 852–869. doi:10.1016/j.ijheatmasstransfer.2016.05.041.
- [12] M.-P. Errera, F. Duchaine, Comparative study of coupling coefficients in Dirichlet–Robin procedure for fluid–structure aerothermal simulations, *Journal of Computational Physics* 312 (2016) 218–234. doi:10.1016/j.jcp.2016.02.022.
- [13] M. B. Giles, Stability analysis of numerical interface conditions in fluid–structure thermal analysis, *International Journal for Numerical Methods in Fluids* 25 (4) (1997) 421–436.
- [14] V. Kazemi-Kamyab, A. Van Zuijlen, H. Bijl, A high order time-accurate loosely-coupled solution algorithm for unsteady conjugate heat transfer problems, *Computer Methods in Applied Mechanics and Engineering* 264 (2013) 205–217.
- [15] A. Monge, P. Birken, On the convergence rate of the Dirichlet–Neumann iteration for unsteady thermal fluid–structure interaction, *Computational Mechanics* 62 (2018) 525–541. doi:10.1007/s00466-017-1511-3.
- [16] V. Kazemi-Kamyab, A. Van Zuijlen, H. Bijl, Analysis and application of high order implicit Runge–Kutta schemes for unsteady conjugate heat transfer: A strongly-coupled approach, *Journal of Computational Physics* 272 (2014) 471–486. doi:10.1016/j.jcp.2014.04.016.
- [17] M.-P. Errera, R. Moretti, R. Salem, Y. Bachelier, T. Arrivé, M. Nguyen, A single stable scheme for steady conjugate heat transfer problems, *Journal of Computational Physics* 394 (2019) 491–502. doi:10.1016/j.jcp.2019.05.036.

- [18] M.-P. Errera, Advanced numerical methods for conjugate heat transfer problems, *Computers & Fluids* (2025) 106594 doi:10.1016/j.compfluid.2025.106594.
- [19] S. Patankar, D. Spalding, A calculation procedure for heat, mass and momentum transfer in three-dimensional parabolic flows, *International Journal of Heat and Mass Transfer* 15 (10) (1972) 1787–1806. doi:10.1016/0017-9310(72)90054-3.
- [20] F. Moukalled, L. Mangani, M. Darwish, *The finite volume method in computational fluid dynamics*, Springer, 2016.
- [21] H. F. Oztop, C. Sun, B. Yu, Conjugate-mixed convection heat transfer in a lid-driven enclosure with thick bottom wall, *International Communications in Heat and Mass Transfer* 35 (6) (2008) 779–785. doi:10.1016/j.icheatmasstransfer.2008.02.003.
- [22] Z. Chen, A. Przekwas, A coupled pressure-based computational method for incompressible/compressible flows, *Journal of Computational Physics* 229 (24) (2010) 9150–9165. doi:10.1016/j.jcp.2010.08.029.
- [23] D. R. Liles, W. H. Reed, A semi-implicit method for two-phase fluid dynamics, *Journal of Computational Physics* 26 (3) (1978) 390–407.
- [24] L. Zhang, A. Kumbaro, J.-M. Ghidaglia, A conservative pressure based solver with collocated variables on unstructured grids for two-fluid flows with phase change, *Journal of Computational Physics* 390 (2019) 265–289. doi:10.1016/j.jcp.2019.04.007.
- [25] M. D. Gunzburger, J. S. Peterson, H. Kwon, An optimization based domain decomposition method for partial differential equations, *Computers & Mathematics with Applications* 37 (10) (1999) 77–93. doi:10.1016/S0898-1221(99)00127-3.
- [26] M. D. Gunzburger, H. K. Lee, An optimization-based domain decomposition method for the Navier-Stokes equations, *SIAM Journal on Numerical Analysis* 37 (5) (2000) 1455–1480. doi:10.1137/S0036142998332864.
- [27] T. Taddei, X. Xu, L. Zhang, A non-overlapping optimization-based domain decomposition approach to component-based model reduction of incompressible flows, *Journal of Computational Physics* 509 (2024) 113038.
- [28] M. Aletti, D. Lombardi, A reduced-order representation of the Poincaré–Steklov operator: an application to coupled multi-physics problems, *International Journal for Numerical Methods in Engineering* 111 (6) (2017) 581–600.
- [29] N. Discacciati, J. S. Hesthaven, Localized model order reduction and domain decomposition methods for coupled heterogeneous systems, *International Journal for Numerical Methods in Engineering* 124 (18) (2023) 3964–3996. doi:https://doi.org/10.1002/nme.7295.
- [30] C. M. Rhie, W. L. Chow, Numerical study of the turbulent flow past an airfoil with trailing edge separation, *AIAA journal* 21 (11) (1983) 1525–1532. doi:10.2514/3.8284.
- [31] F. A. Díaz, E. Castillo, R. C. Cabrales, N. O. Moraga, Non-relaxed finite volume fractional step schemes for unsteady incompressible flows, *Computers & Mathematics with Applications* 146 (2023) 241–252. doi:10.1016/j.camwa.2023.07.002.
- [32] M. D. Gunzburger, J. Lee, A domain decomposition method for optimization problems for partial differential equations, *Computers & Mathematics with Applications* 40 (2000) 177–192. doi:10.1016/S0898-1221(00)00152-8.
- [33] J. Nocedal, S. J. Wright, *Numerical Optimization*, Springer Series in Operations Research and Financial Engineering, 2006. doi:10.1007/978-0-387-40065-5.
- [34] U. Ghia, K. N. Ghia, C. Shin, High-Re solutions for incompressible flow using the Navier-Stokes equations and a multigrid method, *Journal of computational physics* 48 (3) (1982) 387–411. doi:10.1016/0021-9991(82)90058-4.
- [35] M. Vynnycky, S. Kimura, K. Kanev, I. Pop, Forced convection heat transfer from a flat plate: the conjugate problem, *International Journal of Heat and Mass Transfer* 41 (1) (1998) 45–59.
- [36] L. C. Yau, Conjugate heat transfer with the multiphysics coupling library preCICE, Master’s thesis, Technische Universität München (2016).

- [37] J. A. Trapp, R. A. Riemke, A nearly-implicit hydrodynamic numerical scheme for two-phase flows, *Journal of Computational Physics* 66 (1) (1986) 62–82. doi:10.1016/0021-9991(86)90054-9.
- [38] A. J. Chorin, A numerical method for solving incompressible viscous flow problems, *Journal of computational physics* 135 (2) (1997) 118–125.
- [39] J. C. Strikwerda, *Finite difference schemes and partial differential equations*, SIAM, 2004.